*Korean J. Chem. Eng.*, **29**(8), 1025-1037 (2012)
DOI: 10.1007/s11814-011-0275-2

# Analytical investigation of temperature distribution and flame speed across the combustion zones propagating through an iron dust cloud utilizing a three-dimensional mathematical modeling

**Mehdi Bidabadi and Majid Mafi†**

Combustion Research Laboratory, School of Mechanical Engineering,
Iran University of Science and Technology (IUST), Narmak, Tehran 16844, Iran
(*Received 4 July 2010 • accepted 24 October 2011*)

**Abstract**–In the analytical model of iron dust cloud combustion presented in this article, by solving the 3D energy equations, the gas temperature distribution in the channel and a new equation for flame speed are obtained. This equation can determine the relationship between flame speed and particle radius and dust concentration. The equations are written in two limiting cases: lean and rich mixtures. Flame structure consists of preheat, reaction, and post-flame zones for the lean mixture and preheat and reaction zones for the rich mixture. Equations in both mixture conditions are solved using the finite Fourier transform method. By solving the energy equations in each zone and matching the temperature and heat flux at the interfacial boundaries, algebraic equations of flame speed are obtained. The obtained gas temperature distribution in different flame zones in the channel and also flame speed changes in terms of particles' radius, equivalence ratio, and channel width in both lean and rich mixtures are presented in the results section.

Key words: Combustion, Iron Dust Cloud, Laminar Premixed Flame, Lean Mixture, Rich Mixture

## INTRODUCTION

The combustion of particles has been studied in many researches. Premixed filtration combustion of micron and sub-micron particles in the inert porous media has been analyzed theoretically [1]. Also, recently, perfectly volatile particle triple flame has been studied theoretically [2]. A large number of accidental dust explosions have occurred in industrial plants that have powder processing equipment, because more than 70% of powders processed in industry are combustible. Hence, it is crucial to learn as much as possible about the explosion hazards of combustible powders. Many researchers have conducted studies in this field and presented their results in publications [3-11]. In these studies, the focus is mostly on the characteristics of dust explosions, such as the explosion pressure, rate of pressure rise, minimum ignition energy, and explosion concentration limits. Indeed, these data are useful for assessment of explosion hazards of combustible powders. However, not only the results of these studies but also basic knowledge on fundamental phenomena of flame propagation through a combustible particle cloud are necessary in order to take appropriate measures against accidental dust explosions. Therefore, it is indispensable to conduct fundamental studies to explore the mechanisms of flame propagation through a combustible particle cloud. Although there are a few fundamental studies on the mechanisms of flame propagation through particle clouds [12,13], the mechanisms of flame propagation through combustible particle clouds are not clear yet. In particular, when considering metal particles the results are actually ambiguous, becausemetal particles hardly vaporize and there is very little combustible vapor in the gas phase.

†To whom correspondence should be addressed.
E-mail: majid.mafi@gmail.com

Combustion of solid fuels suspended in gases is encountered in a number of applications, such as burning of fossil fuels (e.g. coal), safe handling of flammable dust in industrial settings, and solid-fueled propulsion. Despite their practical importance, a theoretical understanding of dust flames is in an underdeveloped state compared to the well-established theory of homogeneous gas flames. A comprehensive theory of dust combustion is complicated by the enormous diversity of solid fuel properties, as well as the experimental difficulty of creating well-characterized particulate suspensions in the laboratory. The experimental difficulty in generating a uniformlaminar dispersion of dust accounts for the scarcity of fundamental data on dust flame propagation (burning velocity, quenching distance, flame thickness, etc.).

The structure of flames propagating through metal particle clouds and the behavior of metal particles near the flames have been examined experimentally [14,15]. The velocity of particles at the leading edge of combustion zone is nearly proportional to the flame velocity. As the particle diameter becomes larger, the burn-out time becomes much larger than that predicted by the simple analysis.

In another study, the temperature profile across the combustion zone propagating through an iron particle cloud was measured experimentally by a thermocouple to elucidate the propagation mechanism [16]. At the leading edge of the combustion zone, the temperature is about . Near the end of the combustion zone the temperature reaches its maximum value and then decreases. As the iron particle concentration increases, the maximum temperature increases at lower concentration, takes a maximum value, and then decreases at higher concentration. It was found that the propagation velocity has a linear relationship with the maximum temperature.

This result suggests that the conductive heat transfer is dominant in the propagation process of the combustion zone through an iron particle cloud.

The number density profile of particles across a flame propagating through an iron particle cloud has been examined experimentally [17]. The increase in the number density of particles just ahead of the flame will appear not only in iron particle cloud but also in any two-phase combustion systems, such as combustible particle cloud, combustible spray and so on.

Behaviors of particles across upward and downward flame propagating through iron particle clouds have been recorded on photomicrographs by using a high-speed video camera with a microscopic optical system [18]. For upward propagating flame, the maximum value of the number density is about 3.5 times larger than that at the region far ahead of the flame (x>10.0 mm) however, for downward propagating flame, it is only 2.3 times larger than that at the region far ahead of the flame.

Beach et al. [19] presented a model for calculating of burning time of various type of iron nano-particles suspended in air. Clusters containing iron nano-particles (~50 nm in diameter) were found to combust entirely in the solid state due to the high surface to-volume ratio typical of nano-particles. Optical temperature measurements indicated that combustion was rapid (~500 ms) and occurred at relatively low peak combustion temperatures (1,000-1,200 K). Combustion produces a mixture of Fe(III) oxides. X-ray diffraction and gravimetric analysis indicated that combustion was nearly complete (93-95% oxidation). Oxide nano-particles could be readily reduced at temperatures between 673 K and 773 K using hydrogen at 1 atm pressure, and then passivated by the growth of a thin oxide layer.

Performing experiments in a reduced gravity environment can largely eliminate particle sedimentation. The low gravity environment also diminishes buoyancy-induced convectiveflows, permitting very low flame speeds to be observed in suspensions of large particles and slow-burning, nonvolatile fuels. This clear rationale for reduced gravity-based studies of dust flames motivated drop tower experimentation as far back as the 1970s with the work of Ballal [20]. More recently, Dreizen and Hoffmann [9,21] have studied the structure of dust flames in magnesium and aluminum alloy suspensions in a 2.2 sec drop tower. Goroshin, Bidabadi and Lee have obtained quenching distance measurements for two different sizes of aluminum dust in parabolic flight experiments [22].

Most manufacturing units that process nano-particles face a threatfrom fires and explosions. A study examined Ti powders with diameters of 3 μm, 8 μm, 20 μm, 45 μm, 35 nm, 75 nm, and 100 nm, and Fe powders with diameters of 150 μm, 15 nm, 35 nm, and 65 nm [23]. According to the data obtained from the experimental results, the MIEs (minimum ignition energies) for all the nano-powders were less than 1 mJ; the low MIEs of those powders indicated that they are extremely combustible.

Goroshin et al. set up a new experimental apparatus and obtained flame speed and quenching distance measurements of iron dust suspensions in air for a wide range of particle size [24]. Laminar flames propagating in fuel-rich suspensions of iron dust in air were studied in a reduced-gravity environment provided by a parabolic flight aircraft. Equilibrium thermodynamic calculations predict a stoichiometric adiabatic flame temperature in air of 2,230 K (well below the boiling point of iron at 3,130 K), with the products being condensed phase (liquid) $Fe_3O_4$ (83%) and FeO (17%).

In the present study, the iron dust cloud is analyzed as a three-dimensional model. So far, any analytical model has not been presented for an iron dust cloud, and thus our model has novelty in this field. We follow the work of Goroshin et al. [22] and try to solve partial differential equations (PDEs) under two lean and rich mixture conditions. This study takes the initiative in presenting and analytical 3D model of iron dust cloud combustion in a rectangular long channel. Here, heat loss terms to wall are obtained by $[-\lambda(\partial T/\partial y)$ and $-\lambda(\partial T/\partial z)]$, as the boundary conditions.

## MATHEMATICAL MODELING

In the combustion phenomena, there are several parameters and different terms that clearly influence the combustion process. Combustion usually is modeled by differential equations. The main stage in modeling of combustion is to introduce the proper equations that describe the process appropriately. Because of non-linear nature of radiation, radiative heat transfer is neglected for simplicity. Owing to the high temperature of flame zone and post-flame zone, radiation emits from these zones to the lower temperature preheat zone, we assume that radiation is absorbed almost entirely by the channel walls [22].

The analytical model described below is based on a 3D approximation of the flame with conductive heat losses. The main assumptions and approximations are [22] (a) the dust cloud consists of a mixture of gaseous oxidizer and uniformly distributed, equal-sized iron particles, (b) the gravitational effects are neglected, because Goroshin et al., investigated that gravity has no significant effect on the combustion of the iron dust cloud, (c) the particle velocity is equal to the gas velocity in the laminar, steady and uniform flow, and (d) the Biot number for the particle is very small, which implies that the temperature of each particle is uniform, and there is no distribution of temperature within each particle.

### 1. Combustion of a Single Iron Particle

The combustion mechanism of solid iron burning in pure oxygen has been studied [25]. They proposed a model of the iron oxidation process at combustion. The oxidation process consists of the following three steps:

1. A reaction at the oxygen-oxide boundary, which consists of the following elementary steps:

1-a) Oxygen molecules are physically adsorbed on the oxide surface.

1-b) Physically adsorbed oxygen molecules dissociate and the oxygen atoms are chemically adsorbed on particular sites on the oxide surface.

1-c) The chemically adsorbed oxygen atoms are incorporated in the oxide.

2. The diffusion of oxygen ions through the oxide layer.

3. The reaction at the metal-oxide boundary.

Among the above three steps, step (1) is much slower than the other steps.

In their model, an oxygen consumption rate $\dot{m}_O$ is used to express the oxidation reaction rate of iron [15].

$$\dot{m}_O = \Omega P_O^{\beta} T_O^{\gamma} \exp\left(-\frac{E_a}{R_u T}\right) \quad (1)$$

where $\Omega$, $\beta$, and $\gamma$ are constants. $T_O$ is the temperature of oxygen, $P_O$ is the pressure of oxygen. $R_u$ is the universal gas constant, $E_a$ is the activation energy of step (1), and $\dot{m}_O$ is mass consumption rate of oxygen for per unit area at molten oxide surface.

According to their model and experimental results of other stud-

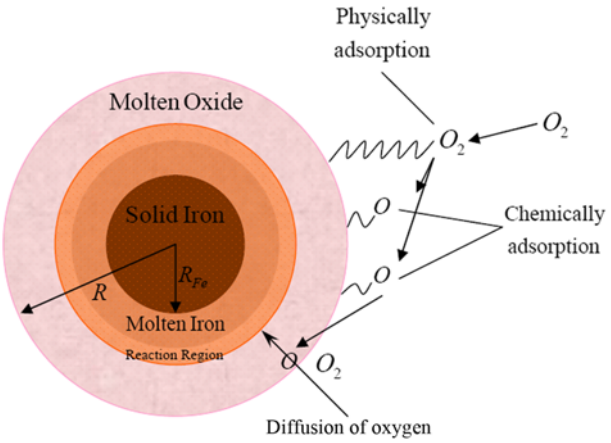


**Fig. 1. Model of single iron particle combustion.**

ies, the combustion model of an individual iron particle can be illustrated as Fig. 1.

The kinetic equation for the heat balance of a particle can be written in the form [19]

$$q+\rho_s\frac{d}{dt}V_s=A_s[\sigma\varepsilon f(T_b^4-T_a^4)+\bar{h}(T_b-T_a)] \quad (2)$$

where $\rho_s$ is the specific density of iron; q is the heat of combustion; $V_s$ is the volume of the particle; $A_s$ is the particle surface area; $T_b$ is the combustion temperature; $T_a$ is the air temperature; $\sigma$ is Boltzmann's constant; $\varepsilon$ is the emissivity; f is a geometric factor determined by the shape of the cluster (pellet or sphere); and $\bar{h}$ is a convective heat transfer coefficient ($\bar{h}$ is proportional to the air pressure, $P_a^{0.8}$).

Disregarding the change of nanoparticle size that occurs in the process of combustion (effectively holding $A_s$ constant), integration of Eq. (2) yields the following formula for the combustion time ($\tau_c$) of a single nanoparticle based on heat balance

$$\tau_c=\frac{\rho_s r Q}{3[\sigma\varepsilon f(T_b^4-T_a^4)+\bar{h}(T_b-T_a)]} \quad (3)$$

where r is the nanoparticle radius. Results obtained from Eq. (3) lead to the same conclusions concerning the combustion time, $\tau_c$, dependence on r, $T_b$, $T_a$, and $\bar{h}$ as those obtained from chemical kinetics where the kinetic equation for the reaction assumes the form

$$\rho_s\frac{d}{dt}V_s=A_sKC_{O_2}^{(2/3)} \quad (4)$$

where K is the effective rate of reaction; and $C_{O_2}$ is the mass concentration of oxygen in the air. Applying the ideal gas equation to determine $C_{O_2}$ and the Arrhenius formula to determine K and integrating Eq. (4), we obtain an expression for the combustion time of a single nanoparticle based on chemical kinetics [19]:

$$\tau_c=\frac{0.825\rho_s r(RT_a)^{0.66}\exp\left(-\frac{E_a}{R_uT_b}\right)}{P_a^{0.66}T_b\Pi^{\delta}} \quad (5)$$

where $R_u$ is the universal gas constant; $E_a$ is the activation energy for oxidation; $P_a$ is air pressure; and $\Pi$ and $\delta$ are constants from the Arrhenius equation for oxidation. Eqs. (3) and (5) describe different processes that take place in nanoparticle combustion.

Toobtain a quantitative understanding of cluster combustion, equations for the combustion of spherical clusters based on heat flow were derived using a method similar to Eq. (3):

$$\tau_{c_{sph}}=\frac{0.182\rho_s r Q}{\sigma\varepsilon f(T_b^4-T_a^4)+\bar{h}(T_b-T_a)} \quad (6)$$

The average convective heat transfer coefficient around iron particles can be calculated from the Whitaker correlation [26]:

$$\bar{h}=\overline{Nu}_d\frac{k}{d} \quad (7)$$

that

$$\overline{Nu}_d=2+(0.4Re_d^{1/2}+0.06Re_d^{2/3})Pr^{0.4}(\mu/\mu_s)^{1/4}$$
$$0.71<Pr<380$$
$$3.5<Re_d<7.6\times10^4$$
$$1<(\mu/\mu_s)<3.2 \quad (8)$$

where k is the conductive heat transfer coefficient, d is the diameter of the iron particle, $\overline{Nu}_d$ is the Nusselt number, $Re_d$ is the Reynolds number on the basis of diameter of particle, Pr is the Prandtl number of surrounding air, $\mu$ is the dynamic viscosity of the air at the bulk temperature of the air, and $\mu_s$ is the dynamic viscosity of the air at the surface temperature of the iron particle. The three conditions mentioned above specify valid ranges for parameters in which the formula is applicable.

The criterion used for determining the type of the mixture is the equivalence ratio. The equivalence ratio, $\phi$, is commonly used to indicate quantitatively whether a fuel-oxidizer mixture is rich, lean or stoichiometric. The equivalence ratio is defined as, $\phi=B/B_{st}$, where B is the dust concentration and $B_{st}$ is the stoichiometric concentration of mixture. The dust concentration, B, equals the total mass of suspended particles per unit volume of space in which particles are dispersed. The stoichiometric concentration of iron dust cloud is $B_{st}\cong0.9$ kg/m$^3$ [16]. If the iron dust concentration is less than 0.9 kg/m$^3$ the mixture is fuel-lean, if the iron dust concentration is more than 0.9 kg/m$^3$ the mixture is fuel-rich, and if the iron dust concentration is equal to 0.9 kg/m$^3$ the mixture is stoichiometric.

## 2. Dust Flame in a Lean Mixture

In the previous study of dust cloud combustion [22], the 1D flame with fuel-lean mixture was assumed to consist of three zones: preheat, flame, and post-flame regimes, as depicted in Fig. 2.

The reaction rate in the preheat zone (zone 1, $-\infty<x<0$) is negligibly small and the gas is heated by conduction from the flame zone. Particles are heated by the surrounding gas until their temperature reaches its ignition point. The difference in temperature between the dust particles and the gas progressively increases due to inertia in the heat exchange. The transient period from ignition to a stable diffusive combustion is much less than the total combustion time $\tau_c$ [22]. In the flame zone, particles are ignited and totally consumed (zone 2, $0<x<v_u\tau_c$). When combustion is completed, the gas temperature gradually returns to the initial value $T_u$ because of heat loss in the post-flame zone (zone 3, $v_u\tau_c<x<+\infty$).

Because of the excess of oxygen in a lean mixture and the weak dependence of oxygen diffusivity on ambient gas temperature, the total particle burning time in a flame front is close to the burning time of a single particle $\tau_c$ [22]. Thus, using the average burning rate of aluminum particle ($m_s/\tau_c$), the heat source term can be written

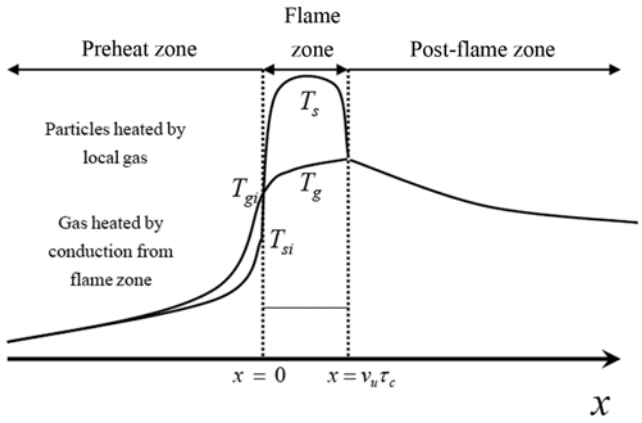


**Fig. 2. 1D flame structure in the fuel-lean mixture.**

for the flame zone as follows [22]:

$$W_f = \frac{B_u}{\tau_c} Q \tag{9}$$

where Q is the heat of reaction per unit mass of fuel. Goroshin et al. [22] (see other examples [27]) also assumed that the particle temperature at the moment of ignition (x=0) is close to the auto ignition temperature of a single particle $T_{si}$ (the ignition temperature in a gas media of constant temperature) and can be found from the equation describing inert particle heating in the preheat zone:

$$v_u m_s c_s \frac{dT_s}{dx} = \frac{\lambda_u}{r}(4\pi r^2)(T_s - T) \tag{10}$$

The gas phase governing equations for mass and energy conservation in 1D approximation can be written as follows:

$$\rho v = \rho_u v_u \tag{11}$$

$$v_u \rho_u c_p \frac{dT}{dx} = \lambda_u \frac{d^2T}{dx^2} + W_f \frac{\rho_u}{\rho} - \kappa \frac{\rho_u}{\rho}(T - T_u) \tag{12}$$

where $\rho$, v, and T are gas density, velocity, and temperature, respectively. $v_u$ stands for the flame speed, $c_p$ for the specific heat capacity of gas at constant pressure, $c_s$ for the specific heat of particle, $W_f$ for the reaction rate characterizing consumption of fuel, r for the particle radius, and $T_s$ for the particle temperature. Index si shows solid particle at the beginning of burning. The third term at the right-hand side of Eq. (12) indicates that the heat loss to the wall is linearly proportional to the temperature difference between the gas and the wall. By solving the energy equation in each zone and matching the temperature and heat flux at the interfacial boundaries, an algebraic equation for the flame speed in a fuel-lean mixture can be found. With this assumption, Goroshin et al. [22] could measure quenching distance, lean flammability limit, and flame speed, but their results did not correspond to the experimental data.

Following the previous 1D works [22,27] andin order to obtain flame speed and temperature distributions, in the present study the flame structure is divided into the three preheat, flame, and post-flame zones. The schematic representation of this structure is in Fig. 3. The x axis in the figure has the opposite direction as that of flame's movement in the channel. Indeed, the coordinate is set on the flame front and the x-direction is toward the right while the flame propagates toward the left. The y axis shows the width of the channel, and the axis displays the depth of the channel.

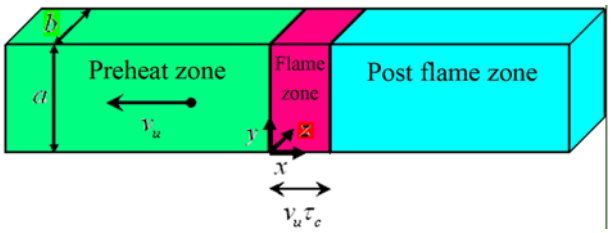


**Fig. 3. The schematic diagram of combustion in a channel with the constant surface temperature under fuel-lean mixture.**

By solving the PDEs of energy in the 3D condition and by using the finite Fourier transform method [28] in all the three zones and satisfying the boundary conditions, we can find an algebraic equation for the flame speed as a function of equivalence ratio. We can also find the lean flammability limit and gas phase temperature distribution. The experimental data show that the quenching plate temperature does not exceed, and is almost equal to, that of the initial or the unburned mixture temperature [20]. Therefore, this temperature is assumed to be constant ($T=T_u$). The thermal conductivity of gas, $\lambda$, which usually varies with temperature, is taken to be constant for the sake of simplicity [29,30]. With these assumptions, the gas phase governing heat diffusivity equation and the boundary conditions for the problem illustrated in Fig. 3 can be obtained.

Preheat Zone

$$\frac{\partial^2 \theta_1}{\partial x^2} + \frac{\partial^2 \theta_1}{\partial y^2} + \frac{\partial^2 \theta_1}{\partial z^2} - 2s\frac{\partial \theta_1}{\partial x} = 0 \tag{13}$$

Flame Zone

$$\frac{\partial^2 \theta_2}{\partial x^2} + \frac{\partial^2 \theta_2}{\partial y^2} + \frac{\partial^2 \theta_2}{\partial z^2} - 2s\frac{\partial \theta_2}{\partial x} = -R\phi \tag{14}$$

Post Flame Zone

$$\frac{\partial^2 \theta_3}{\partial x^2} + \frac{\partial^2 \theta_3}{\partial y^2} + \frac{\partial^2 \theta_3}{\partial z^2} - 2s\frac{\partial \theta_3}{\partial x} = 0 \tag{15}$$

The parameters, $\theta$, s, R, $\phi$ in the above equations are defined as

$$\theta = T - T_u, \quad s = \frac{\rho_u v_u c_p}{2\lambda}, \quad R = \frac{B_{st} Q}{\lambda \tau_c}, \quad \phi = \frac{B}{B_{st}} \tag{16}$$

Boundary conditions

$$\begin{aligned}
&\theta_1(-\infty, y, z) = 0, \quad \theta_1(x, 0, z) = 0, \quad \theta_1(x, a, z) = 0 \\
&\theta_1(x, y, 0) = 0, \quad \theta_1(x, y, b) = 0, \quad \theta_1(0^-, y, z) = \theta_2(0^+, y, z) \\
&\frac{\partial \theta_1}{\partial x}(0^-, y, z) = \frac{\partial \theta_2}{\partial x}(0^+, y, z), \quad \theta_2(x, 0, z) = 0 \\
&\theta_2(x, a, z) = 0, \quad \theta_2(x, y, 0) = 0, \quad \theta_2(x, y, b) = 0 \\
&\theta_2(v_u \tau_c, y, z) = \theta_3(v_u \tau_c, y, z), \quad \frac{\partial \theta_2}{\partial x}(v_u \tau_c, y, z) = \frac{\partial \theta_3}{\partial x}(v_u \tau_c, y, z) \\
&\theta_3(x, 0, z) = 0, \quad \theta_3(x, a, z) = 0, \quad \theta_3(x, y, 0) = 0 \\
&\theta_3(x, y, b) = 0, \quad \theta_3(+\infty, a, z) = 0
\end{aligned} \tag{17}$$

By solving the above equations the following solutions are obtained:

$$\theta_1(x, y, z) = \left(\frac{4}{ab}\right) \sum_{m=1}^{\infty} \sum_{n=1}^{\infty} \{A_{mn} \exp[(s + \sqrt{s^2 + (\mu_m^2 + \lambda_n^2)})x] \times \sin(\mu_m y) \times \sin(\lambda_n z)\} \tag{18}$$

$$\theta_2(x,y,z)=\left(\frac{4}{ab}\right)\times\sum_{m=1}^{\infty}\sum_{n=1}^{\infty}\left\{\left[\begin{array}{l}B_{mn}\exp[(s+\sqrt{s^2+(\mu_m^2+\lambda_n^2)})x]\\+C_{mn}\exp[(s-\sqrt{s^2+(\mu_m^2+\lambda_n^2)})x]\\+\left[\dfrac{((-1)^{m+n+2}+(-1)^{m+1}+(-1)^{n+1}+1)abR\phi}{mn\pi^2(\mu_m^2+\lambda_n^2)}\right]\end{array}\right]\times\sin(\mu_m y)\times\sin(\lambda_n z)\right\} \quad (19)$$

$$\theta_3(x,y,z)=\left(\frac{4}{ab}\right)\sum_{m=1}^{\infty}\sum_{n=1}^{\infty}\{D_{mn}\exp[(s-\sqrt{s^2+(\mu_m^2+\lambda_n^2)})x]\times\sin(\mu_m y)\times\sin(\lambda_n z)\} \quad (20)$$

where

$$\mu_m=\frac{m\pi}{a},\quad \lambda_n=\frac{n\pi}{b}$$

To find parameters $A_{mn}$, $B_{mn}$, $C_{mn}$, and $D_{mn}$, we use boundary conditions described in Eq. (17), which are in the interfacial boundaries of the three zones:

$$A_{mn}=\frac{\left\langle\begin{array}{l}((-1)^{m+n+2}+(-1)^{m+1}+(-1)^{n+1}+1)abR\phi\\\times\left\{\begin{array}{l}(s-\sqrt{s^2+(\mu_m^2+\lambda_n^2)})\\-\left(\begin{array}{l}(s+\sqrt{s^2+(\mu_m^2+\lambda_n^2)})\\\times\exp[(s+\sqrt{s^2+(\mu_m^2+\lambda_n^2)})(v_u\tau_c)]\end{array}\right)\\+\left(\begin{array}{l}2\sqrt{s^2+(\mu_m^2+\lambda_n^2)}\\\times\exp[(s+\sqrt{s^2+(\mu_m^2+\lambda_n^2)})(v_u\tau_c)]\end{array}\right)\end{array}\right\}\end{array}\right\rangle}{\left\langle\begin{array}{l}2mn\pi^2(\mu_m^2+\lambda_n^2)\\\sqrt{s^2+(\mu_m^2+\lambda_n^2)}\\\times\exp[(s+\sqrt{s^2+(\mu_m^2+\lambda_n^2)})(v_u\tau_c)]\end{array}\right\rangle} \quad (21)$$

$$B_{mn}=\frac{((-1)^{m+n+2}+(-1)^{m+1}+(-1)^{n+1}+1)abR\phi(s-\sqrt{s^2+(\mu_m^2+\lambda_n^2)})}{2mn\pi^2(\mu_m^2+\lambda_n^2)\sqrt{s^2+(\mu_m^2+\lambda_n^2)}\exp[(s+\sqrt{s^2+(\mu_m^2+\lambda_n^2)})(v_u\tau_c)]} \quad (22)$$

$$C_{mn}=\frac{((-1)^{m+n+3}+(-1)^{m+2}+(-1)^{n+2}-1)abR\phi(s+\sqrt{s^2+(\mu_m^2+\lambda_n^2)})}{2mn\pi^2(\mu_m^2+\lambda_n^2)\sqrt{s^2+(\mu_m^2+\lambda_n^2)}} \quad (23)$$

$$D_{mn}=\frac{\left\langle\begin{array}{l}((-1)^{m+n+2}+(-1)^{m+1}+(-1)^{n+1}+1)abR\phi\\\times\left\{\begin{array}{l}(s-\sqrt{s^2+(\mu_m^2+\lambda_n^2)})\\-\left(\begin{array}{l}(s+\sqrt{s^2+(\mu_m^2+\lambda_n^2)})\\\times\exp[(s-\sqrt{s^2+(\mu_m^2+\lambda_n^2)})(v_u\tau_c)]\end{array}\right)\\+2\sqrt{s^2+(\mu_m^2+\lambda_n^2)}\end{array}\right\}\end{array}\right\rangle}{\left\langle\begin{array}{l}2mn\pi^2(\mu_m^2+\lambda_n^2)\\\times\sqrt{s^2+(\mu_m^2+\lambda_n^2)}\\\times\exp[(s-\sqrt{s^2+(\mu_m^2+\lambda_n^2)})(v_u\tau_c)]\end{array}\right\rangle} \quad (24)$$

The heat transfer between each particle and surrounding gas is given by [29,30]:

$$\dot{Q}=\bar{h}A_s(T-T_s)=\frac{Nu.\lambda}{2r}(4\pi r^2)(T-T_s)=4\pi r\lambda(T-T_s) \quad (25)$$

Where the Nusselt number is taken as a constant equal to 2. Since the relative velocity between the each particle and ambient gas is assumed zero and the slip velocity is not considered in the modeling, therefore, it is assumed that each particle is suspended in the quiescent gaseous medium. It means that the Reynolds number for the flow around the spherical particles is zero (R=0). In this case, we have Nu=2. Assumingthat each spherical iron particle is immersed in an infinite stagnant fluid, the analytical solution for steady-state conduction is possible and result is expressed in the form Nu=2 [26].

The energy conservation equation for the solid phase is [22,27, 29,30]

$$\frac{\partial\theta_s}{\partial x}=\xi(\theta_1-\theta_s) \quad (26)$$

where

$$\theta_s=T_s-T_u,\quad \xi=\frac{3\lambda}{v_u\rho_s c_s r^2} \quad (27)$$

Boundary condition for Eq. (26),

$$\theta_s(-\infty,y,z)=0 \quad (28)$$

By solving Eq. (26) and using the boundary condition (28), the solid phase temperature of the fuel-lean mixture is obtained as

$$\theta_s(x,y,z)=\left(\frac{4}{ab}\right)\sum_{m=1}^{\infty}\sum_{n=1}^{\infty}\left\{\begin{array}{l}\dfrac{A_{mn}\xi}{(s+\sqrt{s^2+(\mu_m^2+\lambda_n^2)})+\xi}\\\times\exp[(s+\sqrt{s^2+(\mu_m^2+\lambda_n^2)})x]\times\sin(\mu_m y)\times\sin(\lambda_n z)\end{array}\right\} \quad (29)$$

Also, since the particle temperature in x=0 equals the ignition temperature, $T_{si}$, we have

$$\theta_s(0,y,z)=\theta_{si}=\left(\frac{4}{ab}\right)\sum_{m=1}^{\infty}\sum_{n=1}^{\infty}\left\{\frac{A_{mn}\xi}{(s+\sqrt{s^2+(\mu_m^2+\lambda_n^2)})+\xi}\times\sin(\mu_m y)\times\sin(\lambda_n z)\right\} \quad (30)$$

where

$$\theta_{si}=T_{si}-T_u \quad (31)$$

$\theta_{si}$ is expanded as

$$\theta_{si}=\sum_{m=1}^{\infty}\sum_{n=1}^{\infty}\{P_{mn}\sin(\mu_m y)\times\sin(\lambda_n z)\} \quad (32)$$

where (utilizing the orthogonality of functions [28]),

$$P_{mn}=\frac{4((-1)^{m+n+2}+(-1)^{m+1}+(-1)^{n+1}+1)\theta_{si}}{ab\mu_m\lambda_n} \quad (33)$$

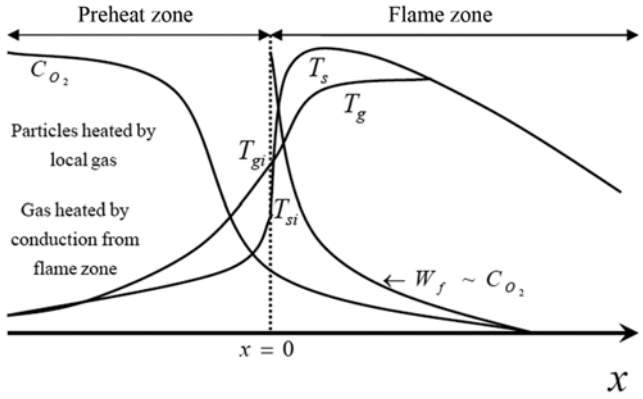


**Fig. 4. 1D flame structure in the fuel-rich mixture.**

In addition (Eqs. (30) and (32)),

$$P_{mn}=\frac{A_{mn}\xi}{(s+\sqrt{s^2+(\mu_m^2+\lambda_n^2)})+\xi} \tag{34}$$

By equating the above two equations (Eqs. (33) and (34)) and after simplifying them, the key equation of flame speed as a function of equivalence ratio is obtained for the 3D condition, which is accurate for each quantity of m and n.

$$\theta_{si}=\frac{A_{mn}\mu_m\lambda_n\xi}{((-1)^{m+n+2}+(-1)^{m+1}+(-1)^{n+1}+1)(s+\sqrt{s^2+(\mu_m^2+\lambda_n^2)}+\xi)} \tag{35}$$

## 3. Dust Flame in a Rich Mixture

The schematic representation of Goroshin et al.'s speculation of the flame structure in a rich dust mixture [22] is presented in Fig. 4. Goroshin and his associates [22] believed that the combustion time of the particle burning in the diffusive regime tended to infinity in stoichiometric or fuel-rich mixtures ($\phi \geq 1$. However, they posited that following the depletion of oxygen, the post-ignition particle burning rate decreases very quickly and gets nearly on the point of 0 at a finite distance from the ignition point. They also assumed the particle radius to be constant and considered the particle burning rate to decrease only as a result of local oxygen concentration changes. In accordance with this assumption, the coefficient $W_f$ in the heat source term in Eq. (12) was written as [22],

$$W_f=\frac{3}{2}\frac{BQ}{\tau_c C_{O_{2_u}}}C_{O_2}(x) \tag{36}$$

where $C_{O_{2_u}}$ is the initial oxygen concentration and $\tau_c$ is the combustion time of an individual particle, which is assumed to have a weak dependence on temperature, and $C_{O_2}(x)$ is the local molar oxygen concentration. The analytical model described below is based on a 3D approximation of the flame with conductive heat losses. To satisfy the energy balance equation, written below, we consider the specific heat to be the sum of the specific heats of the condensed phase and gas [22,31]:

$$\rho_u v_u\left(c_p+\frac{B_u}{\rho_u}c_s\right)\frac{\partial T}{\partial x}=\lambda_u\left(\frac{\partial^2 T}{\partial x^2}+\frac{\partial^2 T}{\partial y^2}\right)+W_f \tag{37}$$

The oxygen conservation equation can be written as [22],

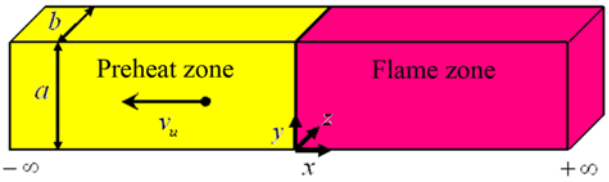


**Fig. 5. The schematic diagram of combustion in a channel with the constant surface temperature under fuel-rich mixture.**

$$\rho_f v_u=\frac{dC_{O_2}(x)}{dx}=D_u\rho_u\frac{d^2C_{O_2}(x)}{dx^2}-\frac{3}{2}\frac{B}{\tau_c C_{O_{2_u}}\Gamma}C_{O_2}(x) \tag{38}$$

where $\Gamma$ is the reaction stoichiometric coefficient. The reaction zone is presumed to be located at x=0. In this section, in order to obtain flame speed and temperature distribution in fuel-rich mixtures, the flame structure is divided into preheat and flame zones, the schematic representation of which is presented in Fig. 5. By solving the partial differential energy equations in the 3D condition using a finite Fourier transform method [28] in both the zones and satisfying the boundary conditions, the algebraic equation for flame speed as a function of equivalence ratio under the fuel-rich mixture condition is obtained.

It is assumed that the coordinate origin is at the bottom corner of the channel cross section at the middle plane, the x axis is towards the flow direction and the y axis is towards the channel width direction, and the z axis is towards of channel depth direction. With these assumptions, the governing heat diffusivity equations and the boundary conditions for the problem illustrated in Fig. 5 can be obtained.

Preheat Zone

$$\frac{\partial^2\theta_1}{\partial x^2}+\frac{\partial^2\theta_1}{\partial y^2}+\frac{\partial^2\theta_1}{\partial z^2}-2s\frac{\partial\theta_1}{\partial x}=0 \tag{39}$$

Flame Zone

$$\frac{\partial^2\theta_1}{\partial x^2}+\frac{\partial^2\theta_1}{\partial y^2}+\frac{\partial^2\theta_1}{\partial z^2}-2s\frac{\partial\theta_1}{\partial x}=-F\exp(M_2x) \tag{40}$$

$$A\frac{dC_{O_2}(x)}{dx}=\frac{d^2C_{O_2}(x)}{dx^2}-A'C_{O_2}(x)$$

The parameters $\theta$, A, A′, $M_1$, $M_2$ and F in equations are defined as

$$\theta=T-T_u,\quad A=\frac{\rho_f v_u}{\rho_u D_u},\quad A'=\frac{3}{2}\frac{1}{\Gamma\rho_u D_u}\frac{B}{\tau_c C_{O_{2_u}}}$$

$$M_1=\frac{1}{2}(A+\sqrt{A^2+4A'}),\quad M_2=\frac{1}{2}(A-\sqrt{A^2+4A'}) \tag{41}$$

$$F=-\frac{3BQ}{2\lambda\tau_c}\frac{A}{A-M_2}$$

Boundary conditions

$$\theta_1(-\infty,y,z)=0,\quad \theta_1(x,0,z)=0,\quad \theta_1(x,a,z)=0$$
$$\theta_1(x,y,0)=0,\quad \theta_1(x,y,b)=0,\quad \theta_1(0^-,y,z)=\theta_2(0^+,y,z)$$
$$\frac{\partial\theta_1}{\partial x}(0^-,y,z)=\frac{\partial\theta_2}{\partial x}(0^+,y,z),\quad \theta_2(x,0,z)=0$$
$$\theta_2(x,a,z)=0,\quad \theta_2(x,y,0)=0,\quad \theta_2(x,y,b)=0$$
$$\theta_2(+\infty,y,z)=0 \tag{42}$$

For oxygen conservation equations we have

Preheat Zone

$$C_{O_2}(x) = C_{O_{2_u}} + c_1 \exp(Ax) \tag{43}$$

Flame Zone

$$C_{O_2}(x) = c_2 \exp(M_2 x) \tag{44}$$

where

$$c_1 = \frac{C_{O_{2_u}} M_2}{A - M_2}, \quad c_2 = \frac{C_{O_{2_u}} A}{A - M_2} \tag{45}$$

By solving the above energy equations the following solutions are obtained:

$$\theta_1(x,y,z) = \left(\frac{4}{ab}\right)\sum_{m=1}^{\infty}\sum_{n=1}^{\infty}\{A_{mn}\exp[(s+\sqrt{s^2+(\mu_m^2+\lambda_n^2)})x] \times \sin(\mu_m y)\times\sin(\lambda_n z)\} \tag{46}$$

$$\theta_2(x,y,z) = \left(\frac{4}{ab}\right) \times \sum_{m=1}^{\infty}\sum_{n=1}^{\infty}\left\{\left[B_{nm}\exp[(s-\sqrt{s^2+(\mu_m^2+\lambda_n^2)})x] + \left[\frac{((-1)^{m+n+2}+(-1)^{m+1}+(-1)^{n+1}+1)Fab}{mn\pi^2(M_2^2-2M_2 s-(\mu_m^2+\lambda_n^2))}\exp(M_2 x)\right]\right] \times \sin(\mu_m y)\times\sin(\lambda_n z)\} \tag{47}$$

where

$$\mu_m = \frac{m\pi}{a}, \quad m = 1, 2, 3, \ldots$$
$$\lambda_n = \frac{n\pi}{b}, \quad n = 1, 2, 3, \ldots \tag{48}$$

Coefficients $A_{mn}$ and $B_{mn}$ are obtained by means of matching the temperature and heat flux at the interfacial boundary between two zones.

$$A_{mn} = \frac{((-1)^{m+n+2}+(-1)^{m+1}+(-1)^{n+1}+1)Fab(M_2 - s + \sqrt{s^2+(\mu_m^2+\lambda_n^2)})}{2mn\pi^2\sqrt{s^2+(\mu_m^2+\lambda_n^2)}(M_2^2-2M_2 s-(\mu_m^2+\lambda_n^2))} \tag{49}$$

$$B_{mn} = \frac{((-1)^{m+n+2}+(-1)^{m+1}+(-1)^{n+1}+1)Fab(M_2 - s - \sqrt{s^2+(\mu_m^2+\lambda_n^2)})}{2mn\pi^2\sqrt{s^2+(\mu_m^2+\lambda_n^2)}(M_2^2-2M_2 s-(\mu_m^2+\lambda_n^2))} \tag{50}$$

Eq. (26) with the boundary condition (28) for the solid phase is applicable here [22], and by solving the equation and employing the boundary condition, the solid phase temperature for the fuel-rich mixture is obtained as

$$\theta_s(x,y,z) = \left(\frac{4}{ab}\right)\sum_{m=1}^{\infty}\sum_{n=1}^{\infty}\left\{\frac{A_{mn}\xi}{(s+\sqrt{s^2+(\mu_m^2+\lambda_n^2)})+\xi} \times \exp[(s+\sqrt{s^2+(\mu_m^2+\lambda_n^2)})x]\times\sin(\mu_m y)\times\sin(\lambda_n z)\right\} \tag{51}$$

Also, as in x=0, the particle temperature is equal to the ignition temperature, $T_{si}$, then we have

$$\theta_s(0,y,z) = \theta_{si} = \left(\frac{4}{ab}\right)\sum_{m=1}^{\infty}\sum_{n=1}^{\infty}\left\{\frac{A_{mn}\xi}{(s+\sqrt{s^2+(\mu_m^2+\lambda_n^2)})+\xi}\times\sin(\mu_m y)\times\sin(\lambda_n z)\right\} \tag{52}$$

$\theta_{si}$ can be expanded in this way

$$\theta_{si} = \sum_{m=1}^{\infty}\sum_{n=1}^{\infty}\{P_{mn}\sin(\mu_m y)\times\sin(\lambda_n z)\} \tag{53}$$

where

$$\theta_{si} = T_{si} - T_u \tag{54}$$

utilizing the orthogonality of functions [28]

$$P_{mn} = \frac{4((-1)^{m+n+2}+(-1)^{m+1}+(-1)^{n+1}+1)\theta_{si}}{ab\mu_m\lambda_n} \tag{55}$$

In addition, based on the above two equations (Eqs. (53) and (54))

$$P_{mn} = \frac{A_{mn}\xi}{(s+\sqrt{s^2+(\mu_m^2+\lambda_n^2)})+\xi} \tag{56}$$

By equating Eqs. (55) and (56) and after simplifying them, the flame speed key relation as a function of equivalence ratio for the 2D condition is obtained as

$$\theta_{si} = \frac{A_{mn}\mu_m\lambda_n\xi}{((-1)^{m+n+2}+(-1)^{m+1}+(-1)^{n+1}+1)(s+\sqrt{s^2+(\mu_m^2+\lambda_n^2)}+\xi)} \tag{57}$$

This relation is relevant to all the m and n values defined above.

## RESULTS AND DISCUSSION

In contrast to gaseous flames that are modeled as a continuum, heterogeneous dust flames consist of individual burning particles that might be at much higher temperature than the surrounding gas. However, if the nondimensional parameter $\chi = \tau_c \alpha / l^2$ (representing the ratio of particle combustion time to inter-particle heat diffusion time, where $l$ is the inter particle spacing and $\alpha$ the thermal diffusivity) is large compared to unity, then a dust flame can still be appropriately modeled as a continuum in which the heat release function is spatially uniform [24]. Estimations for relatively slow burning iron show that this parameter is larger than 5 for fuel-rich mixtures, meaning the "classical"continuum approach to modeling the dust flame structure can be used. The model assumes mechanical equilibration between the particles and the gas (no slip), and the particles are assumed to burn in the diffusive regime after ignition, with the burning rate proportional to the local oxygen concentration. Subsequent quenching of particles due to local oxygen depletion is neglected. The calculated temperature of the gas at the moment of ignition takes into account the dependence of particle ignition temperature on local oxygen concentration as well as the thermal inertia of the particles in the preheat zone. Heat losses to the walls are assumed to be due to molecular heat diffusivity only and are written in volumetric form. The flame speed is then determined by matching the solution for thermal and oxygen flux at the boundary between the preheat and combustion zones. Over the fuel equivalence ratio range

**Table 1. Summary of the thermophysical properties used in the calculations**

| Property | Symbol | Value | Unit | Ref. |
|---|---|---|---|---|
| Density of atmospheric air at 300 K | $\rho_u$ | 1.1614 | kg/m$^3$ | 34 |
| Density of flame at 1,500 K | $\rho_f$ | 0.2322 | kg/m$^3$ | 34 |
| Density of iron at 300 K | $\rho_s$ | 7860 | kg/m$^3$ | 35 |
| Specific heat capacity of atmospheric air at 300 K | $c_p$ | 1007 | J/(kg·K) | 34 |
| Specific heat capacity of iron at 300 K | $c_s$ | 452.38 | J/(kg·K) | 35 |
| Thermal conductivity of atmospheric air at 300 K | $\lambda$ | $26.3\times10^{-3}$ | (W/m·K) | 34 |
| Heat of combustion of iron | Q | 6540 | kJ/kg | 36 |
| Stoichiometric concentration of iron dust cloud | $B_{st}$ | 0.9 | kg/m$^3$ | 16 |
| Total combustion time of a single iron particle with the diameter of 10 micron | $\tau_c$ | 0.02 | s | 19 |
| Initial temperature of unburned mixture | $T_u$ | 300 | K | 16 |
| Ignition temperature of iron particle | $T_{si}$ | 900 | K | 24 |
| Flame speed in the fuel-lean mixture | $v_u$ | 0.12 | m/s | 16 |
| Flame speed in the fuel-rich mixture | $v_u$ | 0.21 | m/s | 16 |
| Width of the channel's cross section | a | 0.1 | m | - |
| Height of the channel's cross section | b | 0.05 | m | - |
| Mass concentration of oxygen in the unburned air | $C_{O_2}$ | 0.271 | kg/m$^3$ | 35 |
| Mass diffusivity of unburned mixture into the flame | $D_u$ | $15.2\times10^{-5}$ | m$^2$/s | 35 |
| Ratio of mass stoichiometric coefficient of iron to air | $\Gamma$ | 3.49 | - | 36 |

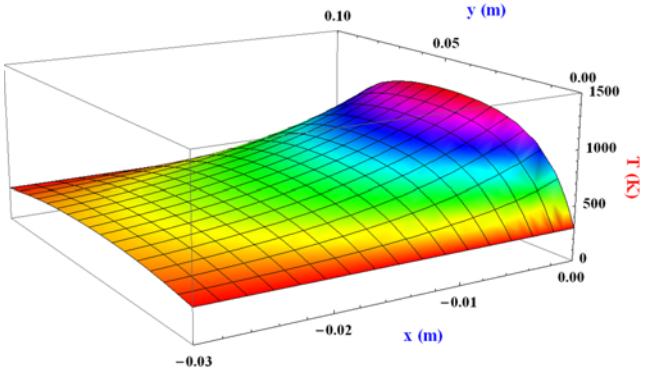


**Fig. 6. Temperature profile of the fuel-lean mixture in the preheat zone in 3D condition ($-\infty<x<0$) at the middle plane of the channel in the z-direction (z=b/2).**

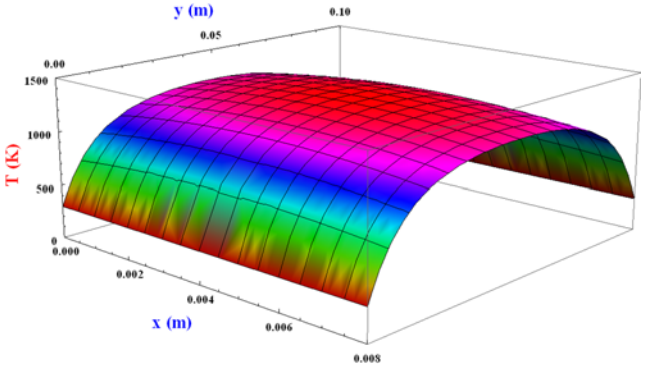


**Fig. 7. Temperature profile of the fuel-lean mixture in the flame zone in 3D condition ($0<x<v_u\tau_c$) at the middle plane of the channel in the z-direction (z=b/2).**

of $\phi$=1.4–1.9, the adiabatic flame temperature, by the THERMO thermodynamic equilibrium code, is predicted to be $T_{af}$=1,810–1,990 K.

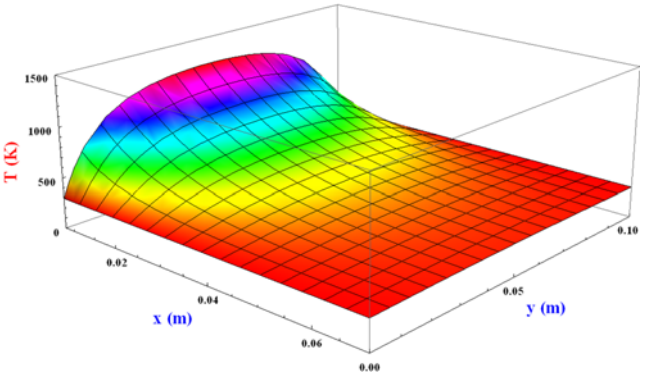


**Fig. 8. Temperature profile of the fuel-lean mixture in the post-flame zone in 3D condition ($v_u\tau_c<x<+\infty$) at the middle plane of the channel in the z-direction (z=b/2).**

The summary of the thermophysical properties used in the calculations and illustrations is listed in Table 1. Figs. 6 to 8 are related to the gas temperature distribution in three preheat, flame, and post-flame zones for the fuel-lean mixture, which are obtained from Eqs. (18) to (20) in the 3D condition. These figures efficiently display the temperature changes in all three zones. The temperature in the middle line of the channel is in accordance with the temperature curves of the experimental models [16]. Heat losses on the channel surface can be obtained using the equation [$-\lambda(\partial T/\partial y)$ and $-\lambda(\partial T/\partial z)$]. In the preheat zone, gas is heated by conduction from the flame zone. In the flame zone, despite the smallness of the zone relative to the other zones, gas temperature change is smaller than the other two lateral zones. In the post-flame zone, the temperature decreases finally down to the initial temperature. With the assumption that the particles are uniformly distributed, temperature profiles are in symmetric relation to the channel center. Temperature distribution for the combustion of iron particles with the diameter of $d_p$=10 μm in

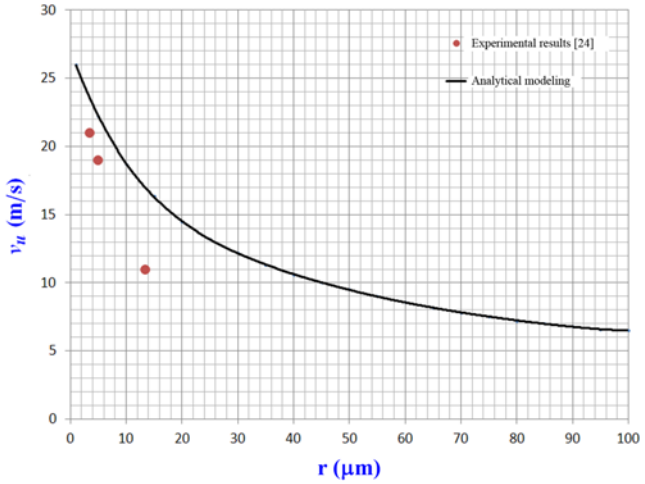


**Fig. 9. Flame speed as a function of particle radius in mixture of iron particle dust and air at a fuel-lean condition of $\phi$=0.6.**

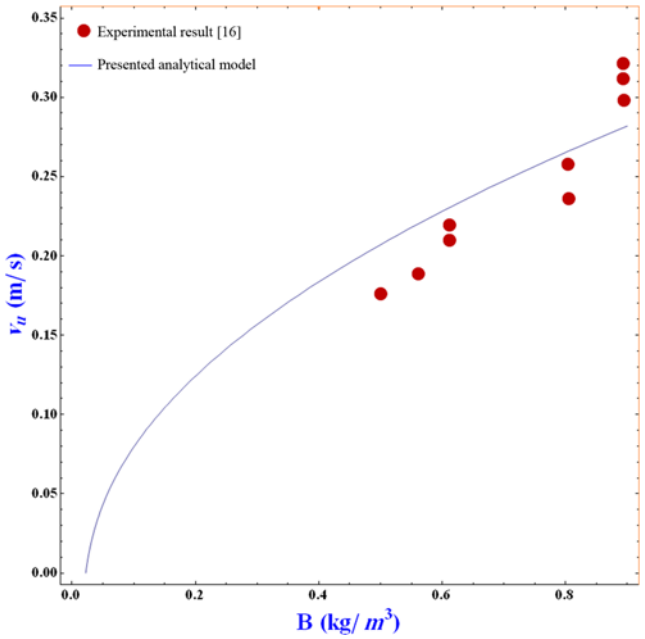


**Fig. 10. Flame speed as a function of dust concentration at a fuel-lean mixture.**

the air and the equivalence ratio $\phi$=0.6 is obtained. Channel width is 10 cm, channel height is 5 cm, and the surface temperature of the channel (in y=0, y=0.1, z=0, z=0.05 m) is equal to the surrounding temperature, as it had been assumed T=$T_u$.

Fig. 9 indicates the calculated 3D laminar flame speed as a function of particle radius for iron-air mixture under fuel-lean conditions (channel width is 10 cm, channel height is 5 cm). The flame speeds increase as particle size decreases [29,30].

Fig. 10 demonstrates the key relation of flame speed in terms of dust concentration for fuel-lean mixture. There is a reasonable agreement between our 3D model and published experimental data [18], a finding that can indicate the effect of 3D solution. In this figure, channel width is 10 cm, channel height is 5 cm and particle diameter is $d_p$=10 μm. In this figure, a lean limit of about 0.02 kg/$m^3$ has

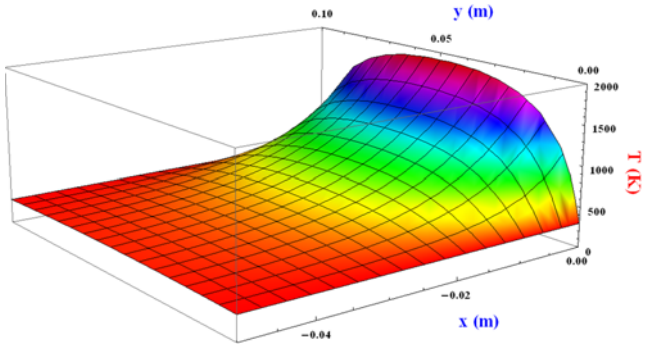


**Fig. 11. Temperature profile of the fuel-rich mixture in the preheat zone in 3D condition (−∞<x<0) at the middle plane of the channel in the z-direction (z=b/2).**

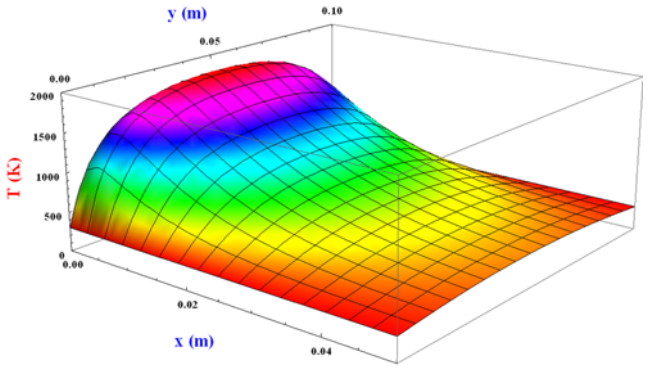


**Fig. 12. Temperature profile of the fuel-rich mixture in the flame zone in 3D condition (0<x<+∞) at the middle plane of the channel in the z-direction (z=b/2).**

been obtained. There is a reasonable agreement between the analytical flame speed results of this study and the experimental results. As can be seen, the 3D model determinesthe lean limit for a higher dust concentration, and the flame speed it shows is lower than the 1D flame speed, i.e., the linear assumption of heat loss term to wall is not much appropriate for the 1D model [20].

Figs. 11 and 12, which are related to the temperature distribution in preheat and flame zones in the fuel-rich mixture, are plotted using Eqs. (48) and (49). These figures illustrate temperature changes in both the zones. In the preheat zone, the particles are heated by the surrounding gas to reach the auto-ignition state. In the flame zone, the temperature decreases finally down to the initial temperature. With the assumption that the particles are uniformly distributed and boundary conditions on the periphery of channel are identical, temperature profiles are in symmetric relation to the center axis of the channel. Temperature distribution for the combustion of iron particles with the diameter of $d_p$=10 μm in the air, and the equivalence ratio $\phi$=1.9 is obtained.

Fig. 13 shows the variation of oxygen concentration across the two zones of combustion in the fuel-rich condition of mixture, which can be derived from Eqs. (43) and (44). The significant relationship of flame speed regarding dust concentration for fuel-rich mixture is sketched in Fig. 14. The flame speed gradually decreases by increasing dust concentration. It is discerned that the 3D new model has proper agreement to the experimental results [24], a finding that

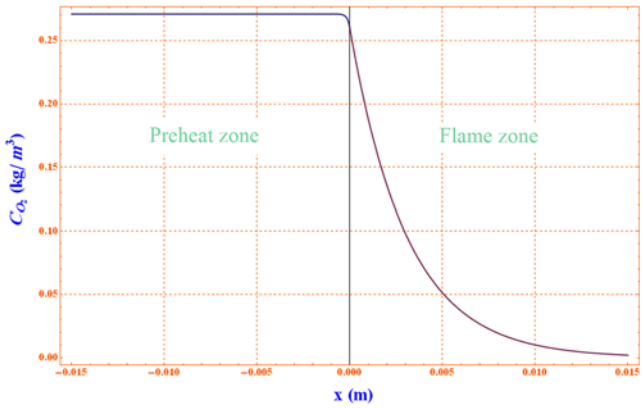


**Fig. 13. Variation of oxygen concentration along the flame at a fuel-rich condition of $\phi$=1.9.**

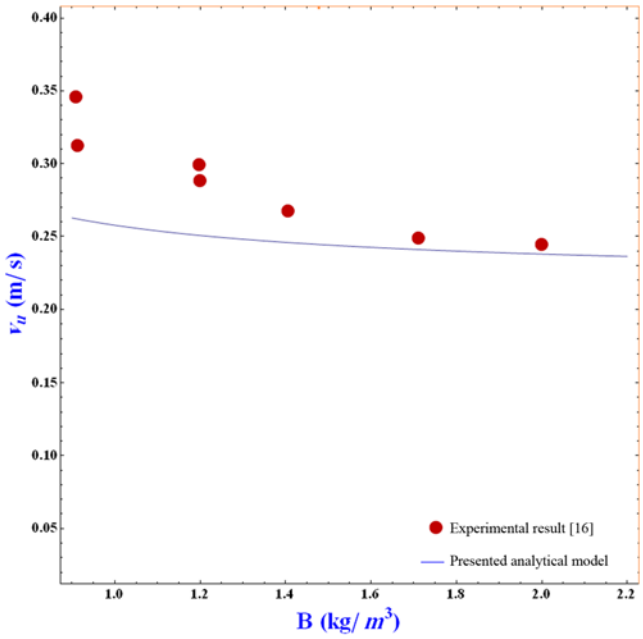


**Fig. 14. Flame speed as a function of dust concentration at a fuel-rich mixture.**

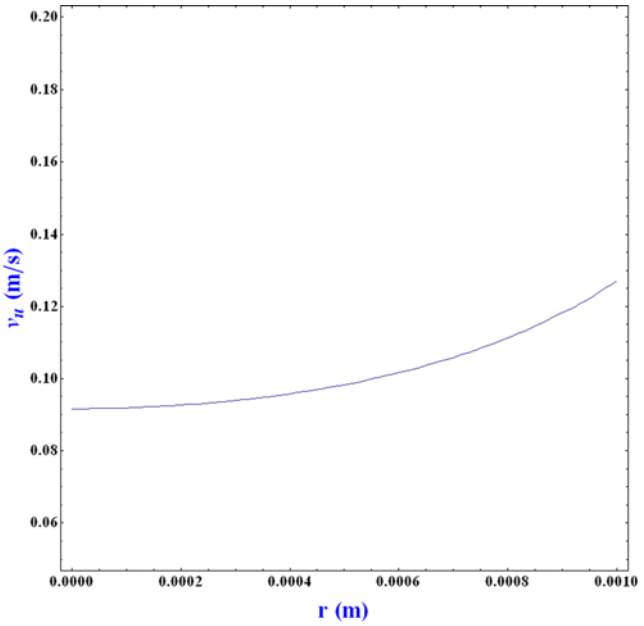


**Fig. 15. Flame speed as a function of particle radius of iron particle dust and air at a fuel-rich condition of $\phi$=1.9.**

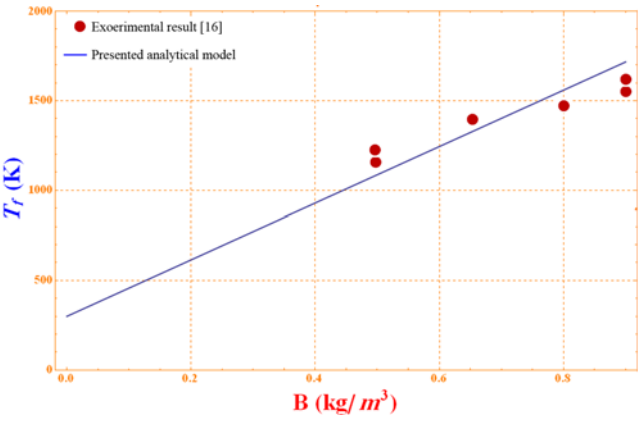


**Fig. 16. Flame temperature as a function of dust concentration at a fuel-lean mixture.**

can indicate the influence of 3D solution. In this figure, channel width is 10 cm, channel height is 5 cm and particle diameter is $d_p$= 10 μm. There is a reasonable agreement between the analytical flame speed results of this studyand the experimental results. Fig. 15 indicates the calculated 3D laminar flame speed as a function of particle radius for iron-air mixtures under fuel-rich conditions (channel width is 10 cm, channel height is 5 cm). The flame speed increases with increasing particle size in the fuel-rich mixture. Based on the assumptions of this study, the flame speed increases gradually with the increase of equivalence ratio in fuel-lean mixture [13]. The variation of flame temperature as a function of dust concentration at fuel-lean mixture is shown in Fig. 16, from which we can see that there is a reasonable consistency between the experimental result and presented analytical result. The dependency of flame temperature on the dust concentration at fuel-rich mixture is presented in Fig. 17. The variation of flame speed versus channel width at fuel-lean mix-

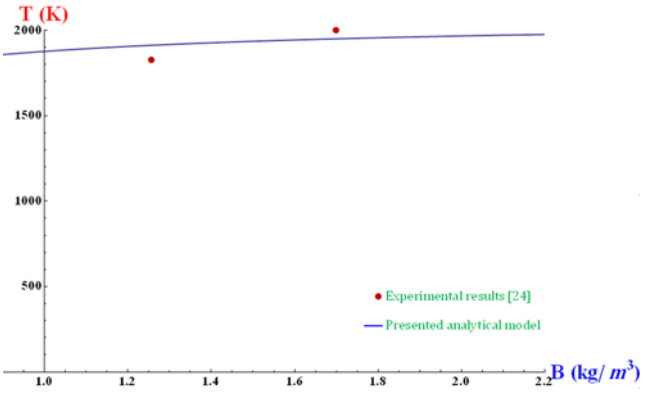


**Fig. 17. Flame temperature as a function of dust concentration at a fuel-rich mixture.**

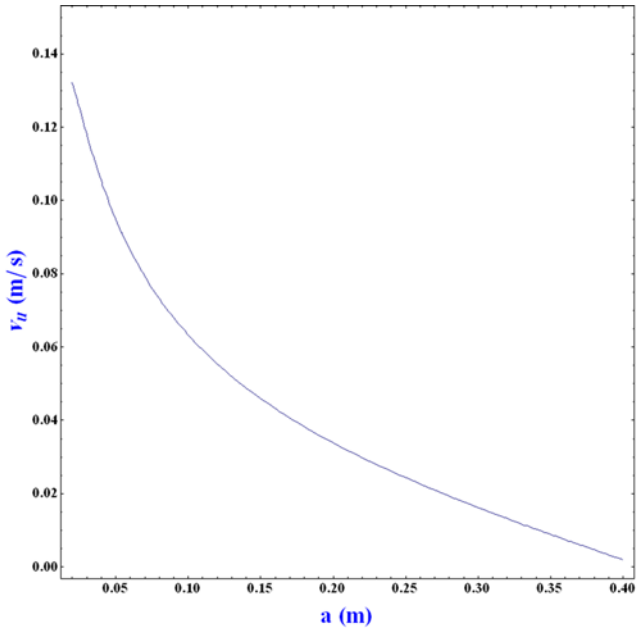


**Fig. 18. Flame speed as a function of channel width at a fuel-lean mixture ($\phi$=0.6).**

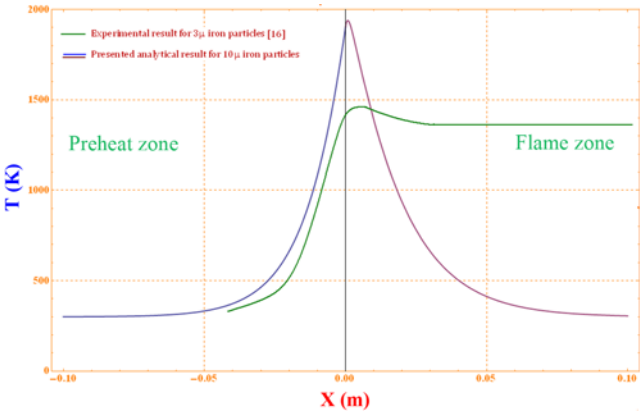


**Fig. 19. The temperature profile across the channel in the fuel-rich mixture.**

ture is plotted in Fig. 18. As depicted there, the flame speed decreases with the increase in channel width. Fig. 19 shows the temperature profile across the channel in the fuel-rich mixture. In general, it is deduced that the tendency of results of the presented analytical modeling (3D) is comparable to the experimental results [16,17,24]. Moreover, results of this study are similar to those of the latest studies in the field of combustion of metallic dust clouds [32,33]. This finding indicates the effect of 3D solution.

## CONCLUSIONS

Combustion of the metal particles suspended in air is a complex phenomenon that has various aspects and factors. To analyzethat process, we have to simplify equations which describe mathematical modeling of process. However, many studies have been performed on hydrocarbon fuel combustion, but few experiments have been done on metallic dust flame, especially on iron particles. Due to the lack of experimental data of iron dust flame, we decided to create an analytical model for iron dust flame to predict combustion phenomena. We could verify some of our results to that of experimental data that are available. But also, we derived a number of analytical expressions that reveal the behavior of iron dust flame. We considered the combustion of iron dust cloud in a long channel whose cross-sectional area is rectangular. We assumed a homogeneous mixture of fine iron particles suspended in air, and particle size and distribution are uniform. We considered that the heat produced inside the channel dissipates and heat loss in peripheral walls of channel to the environment exists. The obtained profile of temperature along the channel shows an increasing trend in the preheat zone from the initial temperature of mixture to the ignition temperature of iron particles, then a gradual increase in temperature in the reaction zone, due to burning of particles completely, and thereafter, a decrease in temperature to the initial temperature. The temperature of the reaction zone indicates theflame temperature of combustion. On the other hand, the flame speed was considered as flame speed in the channel in the modeling. In the lean mixture, the flame speed decreases by increasing the particle radius, which is in accordance with a previous experimental study for iron dust cloud. Also, in the lean mixture, the flame speed increases by increasing the concentration of iron particles in air.

As shown in Figures (10) and (14), the flame speed increases with the increase of dust concentration in the fuel-lean condition. But also, the flame speed decreases gradually with the increase of dust concentration in the fuel-rich condition. This occurrence is justified by the concepts of stoichiometric condition. At the stoichiometric condition in which the equivalence ratio equals to unity, the flame speed becomes a maximum value. In the fuel-lean mixture, by increasing dust concentration, the equivalence ratio increases and approaches to unity thus the flame speed increases and approaches to the maximum value. But in the fuel-rich mixture, by increasing the dust concentration, the equivalence ratio increases and becomes larger than unity therefore, theflame speed decreases and diminishes from the maximum value. However, the flame speed changes based upon particle radius and vice versa in those two conditions. It means that the flame speed decreases by increasing the particle radius in the fuel-lean mixture, and increases by increasing the particle radius in the fuel-rich mixture. It can be observed from the figures that the trend of results of the new analytical model (3D) is similar to the experimental results.

## NOMENCLATURE

x : first coordinate opposite the direction of propagation of flame [m]
y : second coordinate [m]
z : third coordinate [m]
$v_u$ : flame speed [m/s]
$\dot{m}_O$ : oxidation reaction rate of iron [kg/s]
$P_O$ : oxygen partial pressure [Pa]
$T_O$ : temperature of the oxygen [K]
$E_a$ : activation energy [J]
$R_u$ : universal gas constant [kJ/(kmol·K)]
$V_s$ : volume of iron particle [$m^3$]

t : time [s]
$A_s$ : surface area of iron particle [$m^2$]
f : geometric factor determined by the shape of the cluster
$T_b$ : combustion temperature [K]
$T_a$ : air temperature [K]
$\bar{h}$ : average convective heat transfer coefficient around particle [$W/(m^2 \cdot K)$]
r : radius of iron particle [m]
K : effective rate of reaction [$kg^{1/3} \cdot s^{-1}$]
$C_{O_2}$ : mass concentration of oxygen in the air [$kg/m^3$]
$P_a$ : air pressure [Pa]
$\overline{Nu}_d$ : average nusselt number around spherical iron particle
k : thermal conductivity of iron [$W/(m \cdot K)$]
d : diameter of an iron particle [m]
$Re_d$ : reynolds number for air stream around iron particle
Pr : prandtl number for air
$W_f$ : heat source term in energy equation [$W/m^3$]
$B_u$ : initial mass concentration of iron particles in mixture [$kg/m^3$]
Q : heat of combustion of iron [kJ/kg]
$m_s$ : mass of an iron particle [kg]
$c_s$ : specific heat capacity of iron particle [$J/(kg \cdot K)$]
$T_s$ : temperature of iron particle [K]
T : temperature of mixture [K]
v : gas velocity [m/s]
$c_p$ : specific heat capacity of gas at constant pressure [$J/(kg \cdot K)$]
$T_u$ : initial temperature of mixture at entrance of the channel [K]
$B_{st}$ : stoichiometric mass concentration of iron particles cloud [$kg/m^3$]
B : mass concentration of iron particles cloud [$kg/m^3$]
s : defined parameter
R : defined parameter
a : width of infinite rectangular cylindrical channel [m]
b : height of infinite rectangular cylindrical channel [m]
m : counter
n : counter
$A_{mn}$ : fourier coefficient
$B_{mn}$ : fourier coefficient
$C_{mn}$ : fourier coefficient
$D_{mn}$ : fourier coefficient
$\dot{Q}$ : convective heat transfer from gas toiron particle [W]
$T_{si}$ : ignition temperature of iron particle [K]
$P_{mn}$ : fourier coefficient
$C_{O_{2_u}}$ : initial mass concentration of oxygen [$kg/m^3$]
$C_{O_2}(x)$ : local mass concentration of oxygen in the channel [$kg/m^3$]
$D_u$ : diffusivity [$m^2/s$]
A : defined parameter
A′ : defined parameter
$M_1$ : defined parameter
$M_2$ : defined parameter
F : defined parameter
$c_1$ : coefficient
$c_2$ : coefficient

## Greek Letters

$\Omega$ : constant
$\beta$ : constant
$\gamma$ : constant
$\tau_c$ : combustion time of a single iron particle [s]
$\rho_s$ : density of iron particle [$kg/m^3$]
$\sigma$ : stefan-boltzmann constant [$W/m^2 \cdot K^4$]
$\varepsilon$ : emissivity factor
$\Pi$ : constant from arrhenius equation for oxidation
$\delta$ : constant from arrhenius equation for oxidation
$\mu$ : dynamic viscosity of air at bulk temperature of air [Pa·s]
$\mu_s$ : dynamic viscosity of air at surface temperature of iron particle [Pa·s]
$\lambda_u$ : thermal conductivity of air at initial temperature [$W/(m \cdot K)$]
$\rho$ : density of gas [$kg/m^3$]
$\rho_u$ : density of air at initial temperature [$kg/m^3$]
$\kappa$ : coefficient of heat loss [$W/(m^2 \cdot K)$]
$\theta$ : temperature difference of mixture to initial temperature [K]
$\lambda$ : thermal conductivity of mixture [$W/(m \cdot K)$]
$\phi$ : equivalence ratio
$\mu_m$ : eigen value of energy equation
$\lambda_n$ : eigen value of energy equation
$\gamma$ : constant
$\theta_s$ : iron particle temperature minus the initial temperature [K]
$\xi$ : defined parameter
$\theta_{si}$ : ignition temperature of iron particle minus initial temperature [K]
$\rho_f$ : density of mixture in flame zone [$kg/m^3$]
$\Gamma$ : reaction stoichiometric coefficient
$\chi$ : non-dimensional parameter determining continuum

## Subscripts

s : solid particle
O : oxygen
a : air
b : burning
u : unburned
f : flame
1 : preheat zone
2 : flame zone
3 : post flame zone
i : ignition
m : $m^{th}$ value of roots
n : $n^{th}$ value of roots

## REFERENCES


1. M. Bidabadi, J. Fereidooni, R. Tavakoli and M. Mafi, *Korean J. Chem. Eng.*, **28**(2), 461 (2011).
2. M. Bidabadi, Gh. Barari, M. Azimi and M. Mafi, *Int. J. Recent Trend. Eng.*, **1**(5), 26 (2009).
3. W. E. Baker and M. J. Tang, *Gas, dust and hybrid explosions*, Elsevier, New York (1991).
4. K. L. Cashdollar, *J. Loss Prevent. Proc.*, **9**(1), 65 (1996).
5. A. E. Dahoe, J. F. Zevenbergen, S. M. Lemkowitz and B. Scartetl, *J. Loss Prevent. Proc.*, **9**(1), 33 (1996).
6. M. Hertzberg, I. A. Zlochower and K. L. Cashdollar, *24th Symposium (international) on Combustion*, Pittsburgh, PA: The Combustion Institute, 1827 (1992).
7. F. Tamanini and J. V. Valiulis, *J. Loss Prevent. Proc.*, **9**(1), 105

(1996).
8. K. L. Cashdollar, M. Hertzberg and I. A. Zlochower, *22th Symposium (international) on Combustion*, Pittsburgh, PA: The Combustion Institute, 1757 (1988).
9. E. L. Dreizin and V. K. Hoffmann, *Combust. Flame*, **118**, 262 (1999).
10. O. S. Han, M. Yashima, T. Matsuda, H. Matsui, A. Miyake and A. Ogawa, *J. Loss Prevent. Proc.*, **14**(3), 153 (2001).
11. T. Matsuda, M. Yashima, M. Nifuku and H. Enomoto, *J. Loss Prevent. Proc.*, **14**(6), 449 (2001).
12. J. L. Chen, R. Dobashi and T. Hirano, *J. Loss Prevent. Proc.*, **9**(3), 225 (1996).
13. M. Bidabadi and A. Rahbari, *Combust. Explo. Shock+*, **45**(3), 278 (2009).
14. J. H. Sun, R. Dobashi and T. Hirano, *27th Symposium (International) on Combustion*, Pittsburgh, PA: The Combustion Institute, 2405 (1998).
15. J. H. Sun, R. Dobashi and T. Hirano, *Combust. Sci. Technol.*, **150**, 99 (2000).
16. J. H. Sun, R. Dobashi and T. Hirano, *J. Loss Prevent. Proc.*, **14**, 463 (2001).
17. J. H. Sun, R. Dobashi and T. Hirano, *Combust. Flame*, **134**, 381 (2003).
18. J. H. Sun, R. Dobashi and T. Hirano, *J. Loss Prevent. Proc.*, **19**, 135 (2006).
19. D. B. Beach, A. J. Rondinone, B. G. Sumpter, S. D. Labinov and R. K. Richards, *J. Energy Res.-ASME*, **129**, 29 (2007).
20. D. R. Ballal, *Proc R. Soc. Lond. A*, **385**, 21 (1983).
21. E. L. Dreizin, *Combust. Flame*, **105**(4), 541 (1996).
22. S. Goroshin, M. Bidabadi and J. H. S. Lee, *Combust. Flame*, **105**, 147 (1996).
23. H. C. Wu, R. C. Chang and H. C. Hsiao, *J. Loss Prevent. Proc.*, **22**, 21 (2009).
24. F. D. Tang, S. Goroshin, A. Higgins and J. Lee, *Proc. Combust. Inst.*, **32**(2), 1905 (2009).
25. T. Hirano, Y. Sato and K. Sato, *J. Saw. Oxid. Commun.*, **6**, 113 (1984).
26. F. P. Incropera, D. P. De Witt, T. L. Bergman and A. S. Lavine, *Fundamentals of heat and mass transfer*, John Wiley & Sons Inc., New York (2007).
27. S. Goroshin, M. Kolbe and J. H. S. Lee, *Proc. Combust. Inst.*, **28**, 2811 (2000).
28. D. Myint-U and L. Debnath, *Linear partial differential equations for scientists and engineers*, Birkhäuser, Berlin (2007).
29. Y. Huang, G. A. Risha, V. Yang and R. A. Yetter, *Combust. Flame*, **156**(1), 5 (2009).
30. Y. Huang, G. A. Risha, V. Yang and R. A. Yetter, *In Proceedings of the 43rd Aerospace Sciences Meeting and Exhibit*, Reno, Nevada, 10 (2005).
31. S. Goroshin, I. Fomenko and J. H. S. Lee, *Proc. Combust. Inst.*, **26**, 1961 (1996).
32. M. Jadidi, M. Bidabadi and M. E. Hosseini, *P. I. Mech. Eng. G-J Aer.*, **223**, 915 (2009).
33. M. Bidabadi, A. Haghiri and A. Rahbari, *J. Hazard. Mater.*, **176**(1-3), 146 (2010).
34. S. R. Turns, *An introduction to combustion*, McGraw-Hill, Boston (2000).
35. D. W. Green and R. H. Perry, *Perry's chemical engineers' handbook*, McGraw-Hill, New York (2008).
36. T. A. Steinberg, D. B. Wilson and J. M. Stoltzfus, in *Flammability and sensitivity of materials in oxygen-enriched atmosphere*, T. R. William, C. C. Ting and T. A. Steinberg Eds., ASTM Publication, Ann Arbor (1997).
37. M. Bidabadi, *PhD Thesis*, MC Gill University, Canada (1995).
38. V. S. Arpaci, *Conduction heat transfer*, Addison-Wesley, Reading, MA (1966).
39. C. R. Wylie and L. C. Barrett, *Advanced engineering mathematics*, McGraw-Hill, New York (1995).
40. Y. B. Zeldovich, G. I. Barenblatt, V. D. Librovich and G. M. Makhviladze, *The mathematical theory of combustion and explosions*, Consultants Bureau, New York (1985).
41. G. H. Markstain, *AIAA J.*, **1**(3), 550 (1963).
42. A. S. Gordon, C. M. Drew, J. L. Prentice and R. H. Knipe, *AIAA J.*, **6**(4), 577 (1968).